East European Journal of Physics. 4. 491-502 (2024)
DOI:10.26565/2312-4334-2024-4-58 ISSN 2312-4334

FIRST-PRINCIPLES STUDY: THE OPTOELECTRONIC PROPERTIES OF THE WURTZITE ALLOY InGaN BASED SOLAR CELLS, WITHIN MODIFIED BECKE-JOHNSON (MBJ) EXCHANGE POTENTIAL

Amina Benzina[a,b]*, Abdel-Djawad Zebentout[a,b], Lakhdar Benahmedi[c], Taieb Seddik[d], Abdelhadi Lachabi[e], Hamza Abid[e]

[a]*Faculty of Sciences and Technology (FST), University of Ain Temouchent,46000, Algeria*
[b]*Applied Materials Laboratory (AML), Research Center, Djillali Liabes, University of Sidi Bel Abbes, 22000, Algeria*
[c]*Technology and Solids Properties Laboratory, University of Mostaganem Abdelhamid ibn Badis (UMAB), 27000, Algeria*
[d]*Laboratory of Quantum Physics of Matter and Mathematical Modeling (LPQ3M), Faculty of Sciences and Technology, Mustapha Stambouli University of Mascara, 29000, Algeria.*
[e]*Applied Materials Laboratory (AML), Research Center, Djillali Liabes, University of Sidi Bel Abbes, 22000, Algeria*
**Corresponding Author e-mail: benzina.amina@gmail.com, amina.benzina@univ-temouchent.edu.dz*
Received July 20, 2024; revised November 15, 2024; accepted November 18, 2024

Numerical simulation based on Full Potential-Linearized Augmented Plane Wave calculations (FP-LAPW) is implemented in WIEN2K code to study the fundamental structural and optoelectronic properties of the Wurtzite ternary alloy structure InxGa1-xN (x = 0.125, 0.375, 0.625 and 0.875) matched on GaN substrate using a 16-atom supercell. The generalized gradient approximation of Wu and Cohen, the standard local density approach, and the Tran-Blaha modified Becke–Johnson potential was applied to improve the band structure and optical properties of the concerning compounds. Whenever conceivable, we compare the obtained results by experiments and computations performed with diverse computational scheme. In those alloys, the essential points in the optical spectra display the passage of electrons from the valance band to the unoccupied states in the conduction band. The results lead that Becke-Johnson potential will be a promising potential for the bandgaps engineering of III-V compounds which supplied that those materials had crucial absorption coefficients that lead to the application for optoelectronics components, especially solar cells.
Keywords: *Full Potential-Linearized Augmented Plane Wave (FP-LAPW); $In_xGa_{1-x}N$; Tran and Blaha modified Becke-Johnson potential (TB-mBJ); Wurtzite; Solar cells*
PACS: 71.15.m, 71.15.Ap, 71.15.Mb, 71.20.b, 71.55.Eq, 78.20.Ci

1. INTRODUCTION

III-Nitrides elements such as AlN, GaN, InN and their alloys, have all the coveted physical properties for prodigious of tomorrow's optoelectronic devices [1], which developed one of the numerous studied subjects of semiconductors, essentially due to their diverse applications in optoelectronics and high-power/high-temperature electronics.

Significant III-V semiconductors are in the Zinc-blende structure; however, the III-nitrides exist in the Wurtzite phase; though, their metastable Zinc-blende structures were more described and studied [2]. The AlN, GaN and InN crystallize in the stable structure Wurtzite (Wz) [3], this structure is broadly employed because of the band gap nature (direct) in III-nitride semiconductors [4].

In contrast, III-nitrides (III-Ns) have started to accomplish significant consideration toward the photovoltaic application [5]. InN is a suited semiconductor material since its base temperature necessity, enormous carrier mobility and little electron effective mass that affords the application in photovoltaic devices [6]. The band gap of InN was lately found to be 0.7 eV rather than the previous considered 1.3 eV. Since the band gap of $In_xGa_{1-x}N$ comprising the whole spectrum variation, tunable by 0.7 eV for InN to 3.4 eV for GaN. Therefore, permitting the design of multi-junction solar cell with ideal band gap for maximum efficiency [7].

The Wurtzite structure is suitable for growing most III-nitride semiconductors [8]. Growth of $InGaN$ with adequate elevate In incorporation (in fact to attain green emission) has established problematic, while: The lattice mismatch among GaN and InN equal approximate 11% [9]. InN and In-rich $InGaN$ alloys have not been investigated thoroughly because of difficulties associated with the growth of these compound [10]. By expanding the thickness of $InGaN$ layer with high indium (In) content to absorbing light, the material quality turns out to be much more dreadful [11]. Indium gallium nitride ($InGaN$) based alloys are widely applied in the domain of optoelectronics, such as light-emitting diodes (LEDs) and laser diodes (LDs). Recently, $InGaN$-based alloys concerned much research attention in solar cell application [11]. To date, the $InGaN$ heterojunction solar cells using a semi-bulk absorber (multi-layered $InGaN/GaN$ structure) [12]. Textured surface has been performed on $InGaN$-based solar cells [13]. $In_xGa_{1-x}N/GaN$ double heterojunction solar cells [7].

To supplement the existing experimental and theoretical studies and to afford a basis [14] for explaining notions for new components and their applications, the calculations of the structural, electronic properties and the optical spectra of Wz $In_xGa_{1-x}N$ ternary alloys in this framework are presented using first-principles calculations**.**

Cite as: A. Benzina, A.-D, Zebentout, L. Benahmedi, T. Seddik, A. Lachebi, H. Abid, East Eur. J. Phys. 4, 491 (2024), https://doi.org/10.26565/2312-4334-2024-4-58
© A. Benzina, A.-D, Zebentout, L. Benahmedi, T. Seddik, A. Lachebi, H. Abid, 2024; CC BY 4.0 license

The recent theoretical calculations and studies now a day are done utilizing DFT (density functional theory), it has become an important tool in the treatment of many-body problems in atomic, molecular, solid state, and nuclear physics including optical properties of many-body systems [15].

Toward deeper knowledge, slightly extensive experimental and first-principles calculations studies for the ternary alloys $In_xGa_{1-x}N$ with x varying $0 \leq x \leq 1$ have accomplished in the research to perform a significant matching, [4, 16-18]. Therefore, our study could provide as a source of perspective for future searches.

The most prominent interest of DFT lies in its ability to execute computations without empirical parameters as inputs, whose relieves up application exceedingly from constraints set by experiments [19], the first-principles calculations based on DFT was performed in the WIEN2k code [20].

After the introduction, the paper has been arranged in three sections. In Section 2, we concisely illustrate the computational method applied in this study. The important results accomplished for the structural, electronic, and optical properties of $In_xGa_{1-x}N$ ternary alloys are exhibited and discussed in Section 3. Subsequently, the conclusions in Section 4.

2. COMPUTATIONAL DETAIL

The precise and important theoretical solution of the structural, electronic, optical, and magnetic properties of metals and semiconductors is the Kohn-Sham formation [21-23].

The nitrides compounds crystalize in Zinc-blende (space group $F43m$) and Wurtzite structure (space group $P63mc$), Fig. 1 illustrate the stable structure Wurtzite of the binary InN and GaN obtained by the WIEN 2k code.

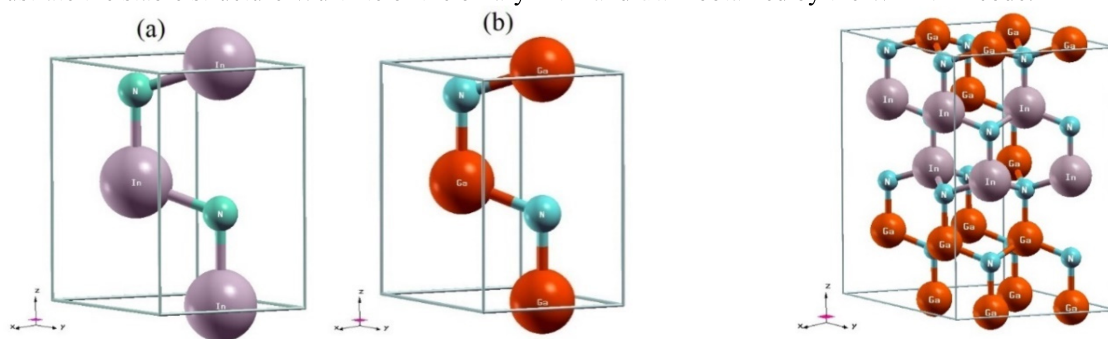

Figure 1. Illustration of a 1×1×1 conventional hexagonal cell- Wurtzite: (a) InN and (b) GaN.

Figure 2. Illustration of a 2×2×2 Wurtzite $In_{0,375}Ga_{0,625}N$ supercell

The current calculations in this study of the physical properties of the Wurtzite ternary alloy $A_xB_{1-x}N$ ($In_xGa_{1-x}N$), so that x signifies In composition, were performed by the FP-LAPW method based on the DFT executed in the WIEN2k package [24]. To model $A_xB_{1-x}N$ Wurtzite alloy, we used a 16-atom $A_nB_{8-n}N_8$ supercell, $(2 \times 2 \times 2)$ that is twice the size of a primitive Wurtzite unit cell in base plane direction [4]. The realized model of crystal structures of ternary $In_xGa_{1-x}N$ alloys is shown in Fig. 2.

The exchange and correlation effects were handled applying three different approximations: the Wu and Cohen Generalized Gradient Approximation (GGA-WC) functional [25,26], the Standard Local Density Approach (LDA), and the Tran and Blaha modified Becke-Johnson exchange potential (TB-mBJ) [25,27,28] is performed to procure a larger band gap value that is generally underestimated by LDA and GGA [25]. For the total and partial Densities Of States (DOS) we considered the orbitals of In ($4d^{10}5s^25p^1$), Ga ($3d^{10}4s^24p^1$) and N ($2s^22p^3$) as valence electrons.

An entirely relativistic calculation moreover scalar relativistic approximation for core and valence state, respectively, without spin-orbit interaction, were employed. In the interstitial region, the plane wave cut-off value of $RMT \cdot K_{max} = 7$ was used [6], where RMT is the minimum radius of the Muffin-Tin spheres are set to 2.04, 1.84, 1.70 atomic units (a.u) for In, Ga and N respectively, and K_{max} provides the magnitude of the largest K vector in the plane wave basis [29]. The maximum l quantum number of the wave function expansion inside the atomic sphere was defined to $l_{max} = 10$ [24], for the Fourier expansion the charge density was extended to $G_{max} = 12\ (a.u)^{-1}$. The Brillion Zone (BZ) integration has been formed applying Monkhorst-Pack Special K-points approach [30].

3. RESULTS AND DISCUSSION

3.1 Structural properties

First, we performed the structural properties of the binary compounds InN and GaN in the both structures Wurtzite (Wz) and Zinc-blende (Zb). The InN and GaN are reported by (1×1×1) conventional hexagonal cell (Wurtzite) and face centered cubic (Zinc-blende).

The computed total energies within GGA as a function of the volume were employed for the perception of theoretical lattice constant and bulk modulus. The equilibrium energy E_0, the Bulk modulus B_0, its first derivative B_0', and the balance volume at zero pressure V_0, by fitting the calculated total energy to the Murnaghan's equation of state (EOS) [31], which is allowed with WIEN2k package.

From Fig. 3 we noticed that the Wz phase was found to be more stable than the Zinc-blende phase for the InN and GaN compounds. The calculated lattice constants and bulk modulus are arranged in Table I.

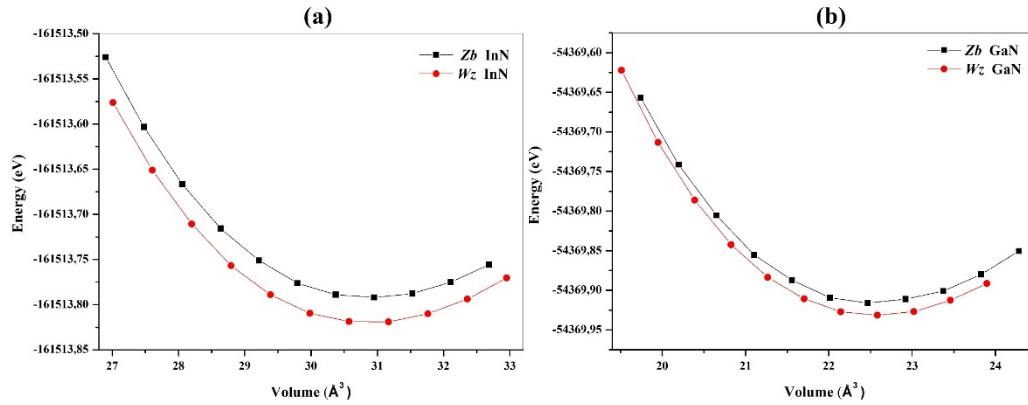

Figure 3. Total energies as a function of volume for the (a) InN and (b) GaN for Zb and Wz phases.

Table I. Lattice constant a and c, bulk modulus B and its first derivative B' of InN and GaN, compared to other experimental or theoretical data, the lattice mismatch $\Delta(a_o)$ and $\Delta(c_o)$ are indicated in the table.

Material	a(Å)			c(Å)			$\Delta(a_o)$	$\Delta(c_o)$	B(GPA)		B'	
	Our	Other	Exp	Our	Other	Exp			Our	Other	Our	Other
InN	3.57	3.59[a]	3.53[a]	5.80	5.78[a]	5.69[a]	0.04	0.11	123.41	--	4.18	--
		3.54[d]	3.51[c]		5.70[d]	5.66[c]	0.06	0.14				
		3.54[f]	3.55[e]		5.71[f]	5.74[e]	0.02	0.06				
GaN	3.21	3.23[a]	3.19[a]	5.24	5.26[a]	5.18[a]	0.02	0.06	176.80	--	4.20	--
		3.18[b]	3.15[c]		5.18[b]	5.14[c]	0.06	0.10				
		3.19[d]	3.18[e]		5.18[d]	5.18[e]	0.03	0.06				
		3.18[f]			5.18[f]							

[a]Ref [32], [b]Ref [33], [c]Ref [34], [d]Ref [35], [e]Ref [36], [f]Ref [37]

The obtained lattice constant parameters a and c for the Wurtzite InN and GaN were somewhat_bigger than the experimental lattice constant parameters, the shift in lattice parameter set as $\Delta(a_o)$ and $\Delta(c_o)$. For further details, no experimental data were possible for the Bulk modulus B_0 and its first derivative B_0'.

The element configuration of ternary alloy $In_xGa_{1-x}N$ acts a notable part in both physical properties and the epitaxial growth process. To study the fundamental structural properties of the ternary alloys $In_xGa_{1-x}N$ matched on GaN substrate for composition of $0 \le x \le 1$, we have considered all studied of the ternary alloys in Wz phase which is the stable compared with Zinc-blende whereas the ternary alloys $In_xGa_{1-x}N$ with 16 atoms with 25% intervals of x.

Reviewing the Vegard's law validity for the Wurtzite ternary alloy $In_xGa_{1-x}N$, the lattice constant is commonly denoted as a linear function depend on x concentration of the compounds. The Vegard's law [38] is applicable for the both a and c lattice parameters as below:

$$a_{In_xGa_{1-x}N} = xa_{InN} + (1-x)a_{GaN}, \tag{1}$$

$$c_{In_xGa_{1-x}N} = xc_{InN} + (1-x)c_{GaN}. \tag{2}$$

The obtained lattice constants of $In_xGa_{1-x}N$ are summarized in Table II, its clearly observed that the lattice constant a and c are in inversely proportional relation with the Indium incorporation.

Table II. Lattice constant a and c calculated by The Vegard's law of $In_xGa_{1-x}N$, compared to other experimental work results.

Materials	a(Å)		c(Å)	
	Our	Exp	Our	Exp
$In_{0,125}Ga_{0,875}N$	3.24	3.20a	5.31	5.21[a]
$In_{0,375}Ga_{0,625}N$	3.33	3.30a	5.45	5.35[a]
$In_{0,625}Ga_{0,375}N$	3.43	3.38a	5.59	5.49[a]
$In_{0,875}Ga_{0,125}N$	3.52	3.47a	5.73	5.64[a]

[a]Ref [4]

3.2 Electronic properties

The energy band gap of a semiconductor is an essential key which is extremely useful for their efficient employment in optoelectronic and different photonic devices. Its small variation can completely modify the utilization in the optoelectronic devices. Therefore, the knowledge of the character of the band gaps of the current materials and their

precise values whether by experiments or calculations are not only significant for their technological applications as well as their band gap tailoring [2].

It is entirely comprehended that the most accurate GGA and LDA undervalue the band gap of semiconductors, the reason is the regardless of the quasiparticle excitations in DFT. To defeat this obstacle, the mBJ approach was employed to produce a band gap approaching the experiment value.

The bandgap energy formula of the $In_xGa_{1-x}N$ is depicted as below:

$$E_g(x) = x \cdot E_g(InN) + (1-x) \cdot E_g(GaN) - b \cdot x \cdot (1-x)\,, \quad (3)$$

where $E_g(x)$, $E_g(InN)$, $E_g(GaN)$ are the bandgap energy for the respective $In_xGa_{1-x}N$, InN and GaN, and b is the bandgap bowing parameter [39], the Vegard's law is convenient for the lattice constants of relaxed $InGaN$. Recent studies propose that the bowing parameter values depend to the indium incorporation, so that for $0 \le x \le 0.5$ the bowing is 1.4 eV, and for $0 \le x \le 1$, the bowing be 1.15 eV or 2.5 eV [4].

Accordingly, the calculated results completed of energy at the point Γ of high-symmetry on the Brillouin zone for the studied binary and ternary compounds using the WC-GGA, LDA, TB-mBJ are summarized in Table III, together with previous experimental results.

Table III. Energy band gap Eg of GaN, InN and $In_xGa_{1-x}N$ calculated with WC-GGA, LDA, TB-mBJ and Vegard's law compared to other experimental or theoretical data.

Materials	Eg (eV)					
	WC-GGA	LDA	TB-mBJ	Vegard's law Calculations		Exp
				bowing 1.11	bowing 2.5	
InN	0.00	0.00	0.77	--	--	0.70[a] – 0.77[b]
$In_{0,125}Ga_{0,875}N$	1.24	1.31	2.58	2.61	2.46	2.88 [b] -3.10 [c]
$In_{0,375}Ga_{0,625}N$	0.49	0.55	1.68	1.91	1.58	1.95 [b]- 2.62 [c]
$In_{0,625}Ga_{0,375}N$	0.03	0.08	1.17	1.35	1.02	1.38 [b]
$In_{0,875}Ga_{0,125}N$	0.00	0.00	0.82	0.93	0.77	0.85 [b]
GaN	1.67	1.75	3.01	--	--	3.50[a] -3.42[b]- 3.42[c]

[a] Ref [16]. [b] Ref [4]. [c] Ref [18].

It is obviously noticed that the calculated band gap values (Table III) with TB-mBJ display a clear improvement over the previously calculated values using Vegard's law.

Fig. 4 present the band structure of the considered ternary alloy $In_xGa_{1-x}N$, the high-symmetry lines through the first irreducible Brillouin zone estimated within mBJ approach.

The Valance Band Maximum (VBM) and the Conduction Band Minimum (CBM) appear at the Γ point showing that the studying materials have a direct band gap. Those results correspond properly through the precedent experimental and theoretical searches.

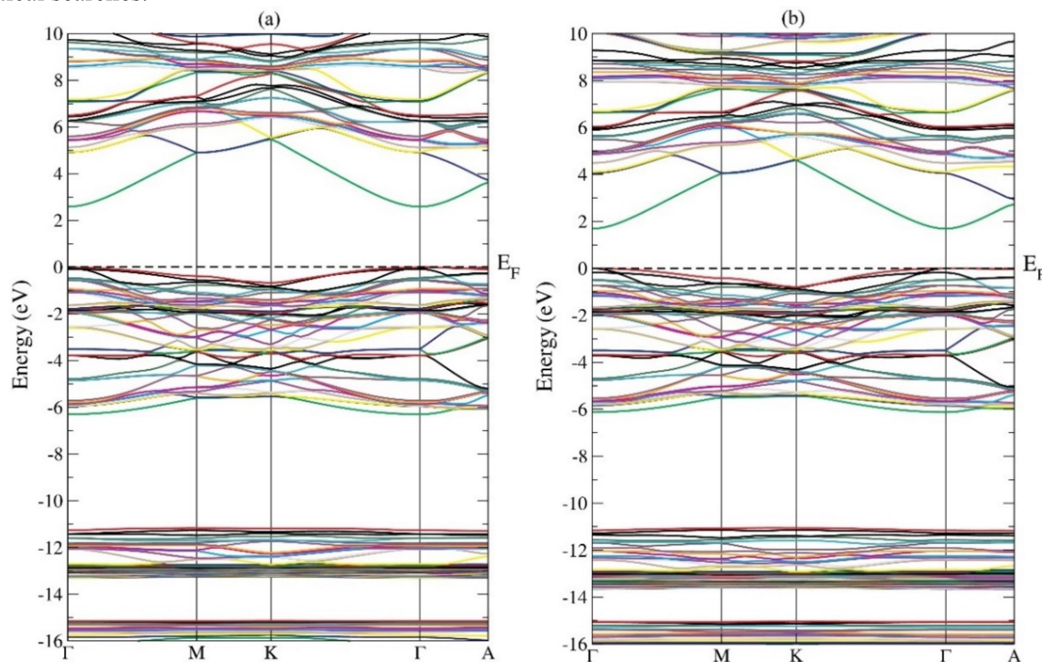

Figure 4. Band structures within TB-mBJ for (a)$In_{0,125}Ga_{0,875}N$, (b) $In_{0,375}Ga_{0,625}N$,(c) $In_{0,625}Ga_{0,375}N$ and (d) $In_{0,875}Ga_{0,125}N$

(continued on the next page)

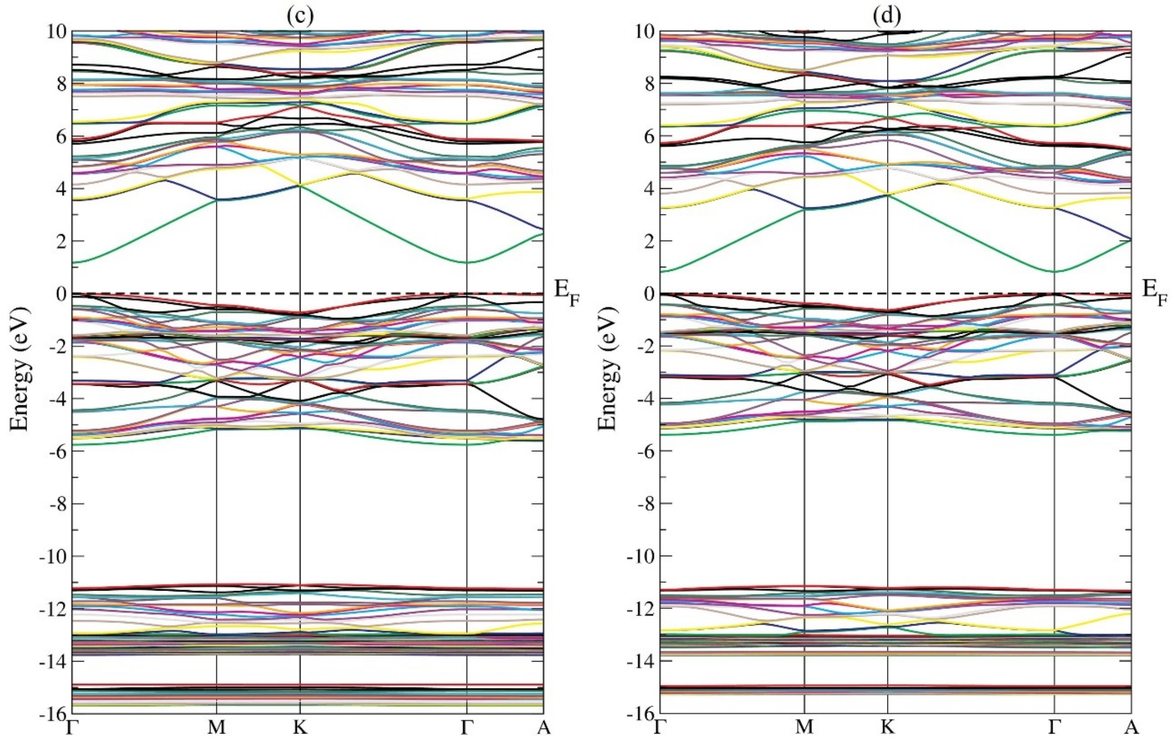

Figure 4. Band structures within TB-mBJ for (a)$In_{0,125}Ga_{0,875}N$, (b) $In_{0,375}Ga_{0,625}N$,(c) $In_{0,625}Ga_{0,375}N$ and (d) $In_{0,875}Ga_{0,125}N$.

The data of energy band gap using the WC-GGA, LDA and TB-mBJ approximations depicted in Table III are plotted in Fig. 5.

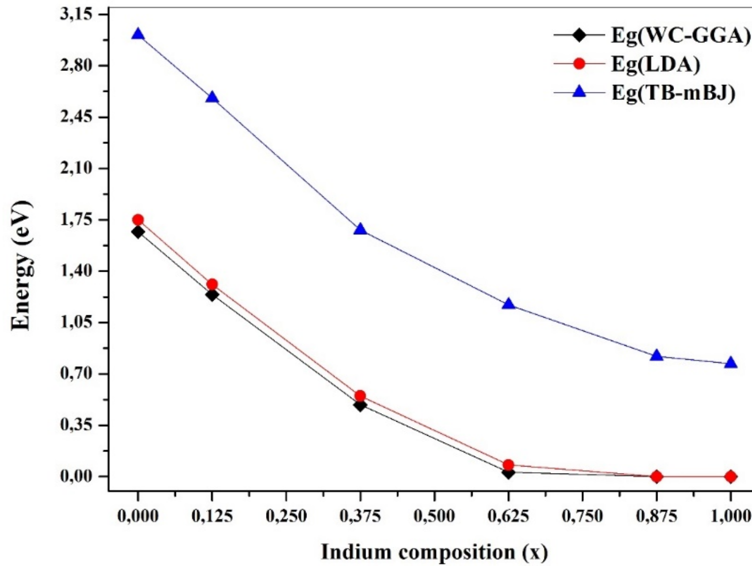

Figure 5. Band gap energy as a function of Indium concentration.

This last one displays that at small Indium composition, a notable bowing can be achieved however at huge indium composition, the bowing could be negligible.

Therefore, the Band gap energy can be characterized as a function of the Indium composition, the Eg is fitted and expressed by the following equations:

$$Eg^{WC-GGA}(x) = 1.68 - 4.13x + 2.46x^2, \tag{4}$$

$$Eg^{LDA}(x) = 1.76 - 4.15x + 2.39x^2, \tag{5}$$

$$Eg^{TB-mBJ}(x) = 3.03 - 4.25x + 1.98x^2. \tag{6}$$

These equations are related to the formula (3), where the bowing b = 2.46, 2.39 and 1.98 corresponding the respective approximations WC-GGA, LDA and Tb-mBJ.

The information of the electron density of states (DOS) is wanted to comprehend and simplify, the calculated band structure to know the contributing atomic states, the total and the partial DOS of the studied ternary $In_{0,125}Ga_{0,875}N$, $In_{0,375}Ga_{0,625}N$, $In_{0,625}Ga_{0,375}N$ and $In_{0,875}Ga_{0,125}N$ respectively are plotted in Fig. 6, which are estimated using the TB-mBJ scheme. We have considered the inner-shell electrons in the valence electrons of In ($4d^{10}5s^{2}5p^{1}$), Ga ($3d^{10}4s^{2}4p^{1}$), and N ($2s^{2}2p^{3}$) shells [40].

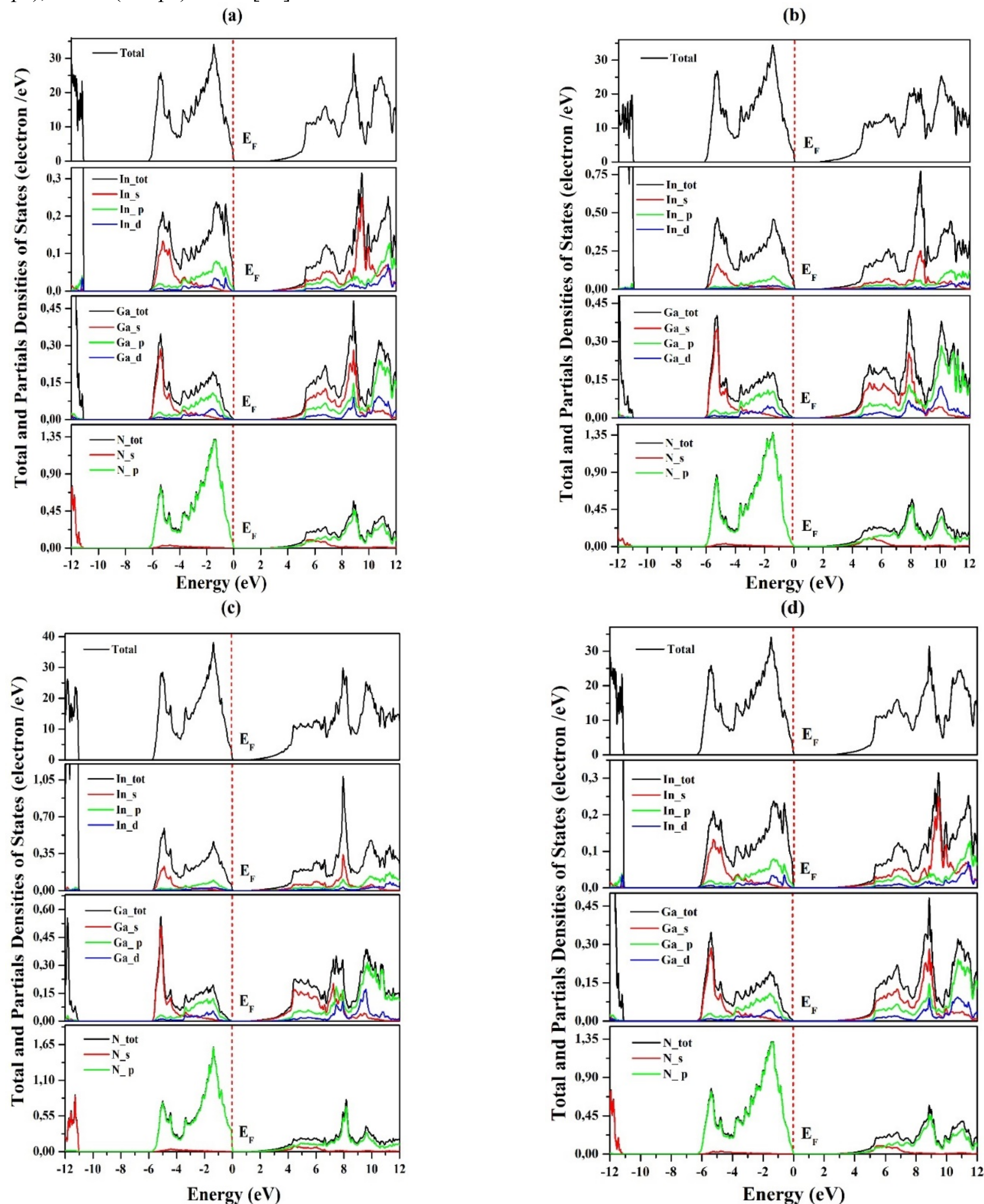

Figure 6. Total and partial densities of states for (a) $In_{0,125}Ga_{0,875}N$, (b) $In_{0,375}Ga_{0,625}N$, (c) $In_{0,625}Ga_{0,375}N$ and (d) $In_{0,875}Ga_{0,125}N$ compounds

It is obviously shown from Fig. 6, the state's lesser E_F the valence band be divided by two region the narrow range between -13.08 eV to -11.06 eV, mainly originates from the hybridization of In s/p, Ga s/p and N /s states. The wider region from -6.08 eV to Fermi level contain two peaks, the first between -6.08 to -4.10 eV is mainly occupied by N /p, Ga /s and In /s states while the second from -4.10 eV approaching to fermi level is densely dominated by N /p, Ga P/d and In p/d states.

The studied ternary compounds note a definite energy gap among the valance and the conduction energy bands of 2.58, 1.68, 1.17 and 0.82 eV for the $In_{0,125}Ga_{0,875}N$, $In_{0,375}Ga_{0,625}N$, $In_{0,625}Ga_{0,375}N$ and $In_{0,875}Ga_{0,125}N$ respectively, the alloys system preserving its semiconductor character. Hence, the dominant conduction electron states possess a composition from several N /p, Ga s/p/d and In s/p.

3.3 Optical properties

The optical properties are straightly correlated to the electronic band gap of a semiconductor, characterizing the interaction of electromagnetic radiations with a material. The dielectric function $\varepsilon(\omega)$ acts an essential part in exploring the optical properties of a compound.

To provide an excellent optical properties of the WZ semiconductors, a 480 *k*-points was achieved into the irreducible part of Brillouin zone *(BZ)* integration using the TB-mBJ exchange potential for the $In_{0,125}Ga_{0,875}N$, $In_{0,375}Ga_{0,625}N$, $In_{0,625}Ga_{0,375}N$ and $In_{0,875}Ga_{0,125}N$.

The dielectric function can be written as $\varepsilon(\omega) = \varepsilon_1(\omega) + i\varepsilon_2(\omega)$, illustrates the material response to the photon spectrum, where the imaginary part of the dielectric function $\varepsilon_2(\omega)$ signifies the optical absorption in the crystal, those able to acquire from the momentum matrix elements through the occupied and unoccupied eigenstates. It signifies the diversity of inter-band transitions in a semiconductor and the real part $\varepsilon_1(\omega)$ of the dielectric function is related to the imaginary part $\varepsilon_2(\omega)$ by employing the Kramers Kronig (KK) relations [41].

$$\varepsilon_1(\omega) = 1 + \frac{2}{\pi} P \int_0^{\infty} \frac{\acute{\omega}\varepsilon_2(\acute{\omega})}{\acute{\omega}^2 - \omega^2} d\acute{\omega}. \tag{7}$$

Different optical properties can be determined from the dielectric function, selected the refractive index $n(\omega)$, the extinction coefficient $k(\omega)$, the reflectivity $R(\omega)$, and the absorption coefficient $\alpha(\omega)$, within the following relations [42]:

$$n(\omega) = \sqrt{\frac{|\varepsilon(\omega)| + \varepsilon_1(\omega)}{2}}, \tag{8}$$

$$K(\omega) = \sqrt{\frac{|\varepsilon(\omega)| - \varepsilon_1(\omega)}{2}}, \tag{9}$$

$$R(\omega) = \frac{(n(\omega)-1)^2 + k(\omega)^2}{(n(\omega)+1)^2 + k(\omega)^2}, \tag{10}$$

$$\alpha(\omega) = \frac{4\pi}{\lambda} k(\omega). \tag{11}$$

Where, λ is the wavelength of light in the vacuum.

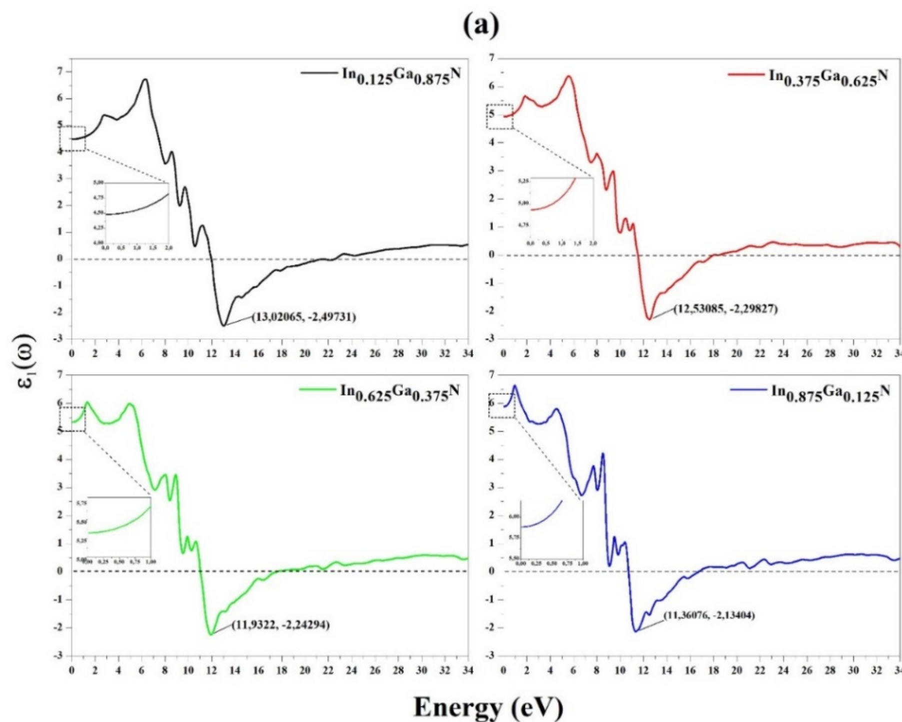

Figure 7. Real part ***ε1(ω)*** (a) and imaginary part *ε2(ω)* (b) for $In_{0,125}Ga_{0,875}N$, $In_{0,375}Ga_{0,625}N$, $In_{0,625}Ga_{0,375}N$ and $In_{0,875}Ga_{0,125}N$

(continued on the next page)

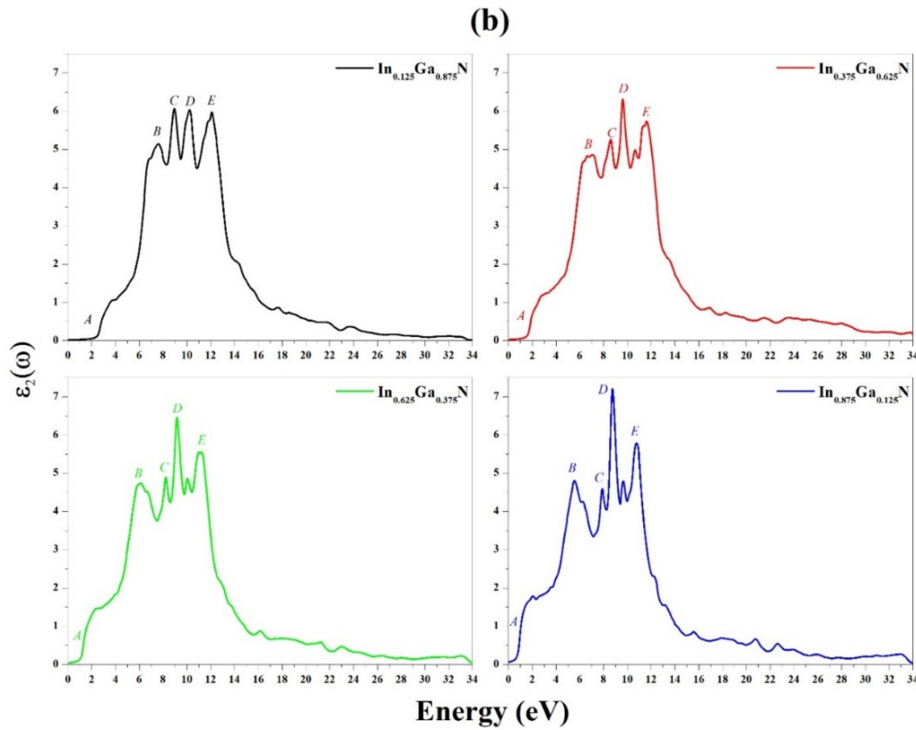

Figure 7. Real part ***ε1(ω)*** (a) and imaginary part *ε2(ω)* (b) for $In_{0,125}Ga_{0,875}N$, $In_{0,375}Ga_{0,625}N$, $In_{0,625}Ga_{0,375}N$ and $In_{0,875}Ga_{0,125}N$

Fig.7 (a) show the real part of dielectric function $\varepsilon_1(\omega)$, afford the static dielectric constant $\varepsilon_1(0)$ presented in Table IV. The inversely proportional relation between the $\varepsilon_1(0)$ and E_g can be defined by the Penn model [43],

$$\varepsilon \approx 1 + (\hbar\omega_p/E_g)^2. \tag{12}$$

Where, ω_p is the plasma frequency, and $\hbar = h/2\pi$ (h is the Planck constant).

Table IV. Collected the peak positions of *ε2(ω)*, static dielectric constant *ε1(0)*, refractive index *n(0)* and Static reflectivity *R(0)* for $In_{0,125}Ga_{0,875}N$, $In_{0,375}Ga_{0,625}N$, $In_{0,625}Ga_{0,375}N$ and $In_{0,875}Ga_{0,125}N$.

Materials	Critical points					Static dielectric constant	Static refractive index	Static reflectivity
	A	*B*	*C*	*D*	*E*	*ε1(0)*	*n(0)*	*R(0)*
$In_{0,125}Ga_{0,875}N$	2.58	7.55	8.93	10.22	12.05	4.49	2.11	0.128
$In_{0,375}Ga_{0,625}N$	1.68	7.07	8.64	9.60	11.65	4.93	2.22	0.144
$In_{0,625}Ga_{0,375}N$	1.17	6.06	8.24	9.19	11.11	5.33	2.30	0.156
$In_{0,875}Ga_{0,125}N$	0.82	5.56	7.89	8.71	10.75	5.88	2.42	0.172

$\varepsilon_1(\omega)$ rises within a small energy margin, then decreases for values less than one, the lower values of $\varepsilon_1(\omega)$ occurs at 13.02, 12.53, 11.93 and 11.36 eV for the $In_{0,125}Ga_{0,875}N$, $In_{0,375}Ga_{0,625}N$, $In_{0,625}Ga_{0,375}N$ and $In_{0,875}Ga_{0,125}N$, respectively. These values correspond to the higher values of the reflectivity shown in Fig.7 (a). Furthermore, when $\varepsilon_1(\omega)$ attains a stability when getting energy more than (>22, 18, 17and 16) eV for the respective ternary $In_{0,125}Ga_{0,875}N$, $In_{0,375}Ga_{0,625}N$, $In_{0,625}Ga_{0,375}N$ and $In_{0,875}Ga_{0,125}N$, designating that the incident photons cross the material without any notable interaction.

From Fig.7 (b), the calculated $\varepsilon_2(\omega)$ spectra reveal that the first crucial point A, further set as optical's absorption edge occurs at 2.58 eV, 1.68 eV, 1.17 eV and 0.82 eV which represent the direct optical transitions for the respective compounds $In_{0,125}Ga_{0,875}N$, $In_{0,375}Ga_{0,625}N$, $In_{0,625}Ga_{0,375}N$ and $In_{0,875}Ga_{0,125}N$. The electronic optical transitions (represented by peaks B, C, D and E given in Table IV among the valence band and conduction band at Γ_{15v}- Γ_{1c} symmetry point, originate the absorption region.

As provides in Fig. 8 (a), the reflectivity reached the maximum in the photon energy range (12.53 to 16.55) eV, (11.84 to 15.40) eV, (11.51 to 15.06) eV and (10.88 to 14.56) eV for the compounds $In_{0,125}Ga_{0,875}N$, $In_{0,375}Ga_{0,625}N$, $In_{0,625}Ga_{0,375}N$ and $In_{0,875}Ga_{0,125}N$,respectively.

This Prominent reflectance is explained to the resonance plasmon rising in the Ultraviolet range. Furthermore, the In integration decrease proportionally the maximum value of the reflectivity as below 0.48, 0.46, 0.45 and 0.44 (a.u) for the respective In concentration ($x = 0.125$, 0.375, 0.625 and 0.875).

The refractive index follows the pattern of $\varepsilon_1(\omega)$, It is seen from the Fig.8(b) that $n(\omega)$ spectra increase and reach a peak value of 2.67 at 6.48 eV , 2.60 at 5.72 eV, 2.52 at 5.23 eV and 2.57at 0.93 eV for the respective $In_{0,125}Ga_{0,875}\,N$, $In_{0,375}Ga_{0,625}\,N$, $In_{0,625}Ga_{0,375}\,N$ and $In_{0,875}Ga_{0,125}\,N$ compounds. Beyond the maximum, the spectra decrease inferior to 1. As the bandgap is decreased when we increase the In amount, while $n(0)$ alter vice versa with the band gap of the compounds as mentioned in the Table III. The Refractive index inferior than unity ($vg = c/n$) exhibits that the group velocity of the incident radiation is bigger than the lightspeed c [44,45]. It signifies that the group velocity shift to negative domain and the material turn into superluminal for high energy photons.

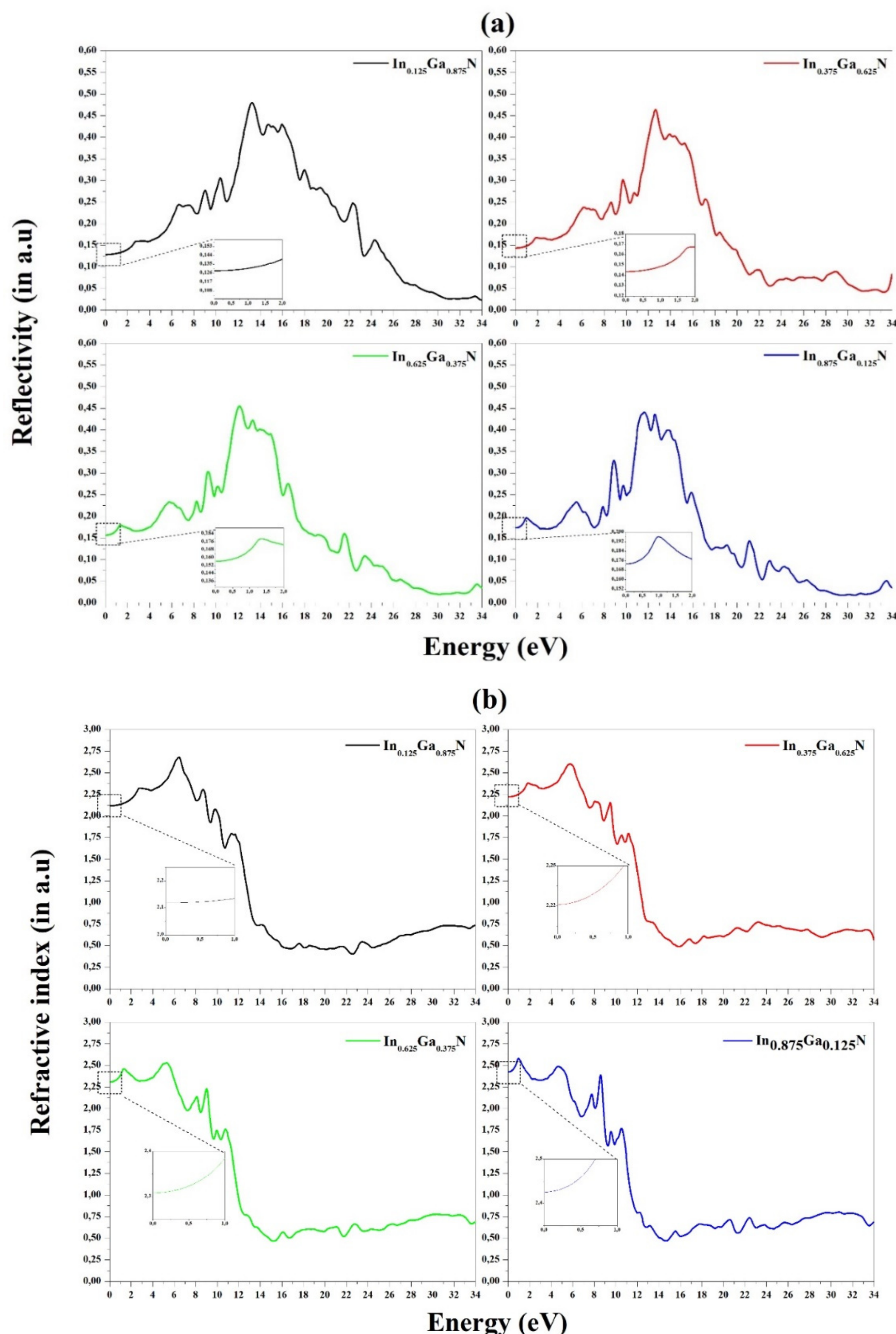

Figure 8. Reflectivity $R(\omega)$ (a) and (b) Refractive index $n(\omega)$ for $In_{0,125}Ga_{0,875}\,N$, $In_{0,375}Ga_{0,625}\,N$, $In_{0,625}Ga_{0,375}\,N$ and $In_{0,875}Ga_{0,125}\,N$.

It is clearly from the absorption $\alpha(\omega)$ spectra plotted in Fig. 9, that the absorption edge occurs at the energy values 2.58, 1.68, 1.17 and 0.82 eV for the compounds $In_{0,125}Ga_{0,875}\,N$, $In_{0,375}Ga_{0,625}\,N$, $In_{0,625}Ga_{0,375}\,N$ and

$In_{0,875}Ga_{0,125}\,N$, respectively. These previous values are identical to the energy gaps of $\Gamma v - \Gamma c$. The absorption coefficient is the most important characterizing the solar cells, the maximum $\alpha(\omega)$ is 248.41, 231.96, 219.30 and 211.55 for In concentration of ($x = 0.125$, 0.375, 0.625 and 0.875), therefore confirm [46] study, that for In poor region (x less or equal 25%) of the $In_xGa_{1-x}N$ may allow the possibility of appropriate bandgap engineering for solar cell utilization.

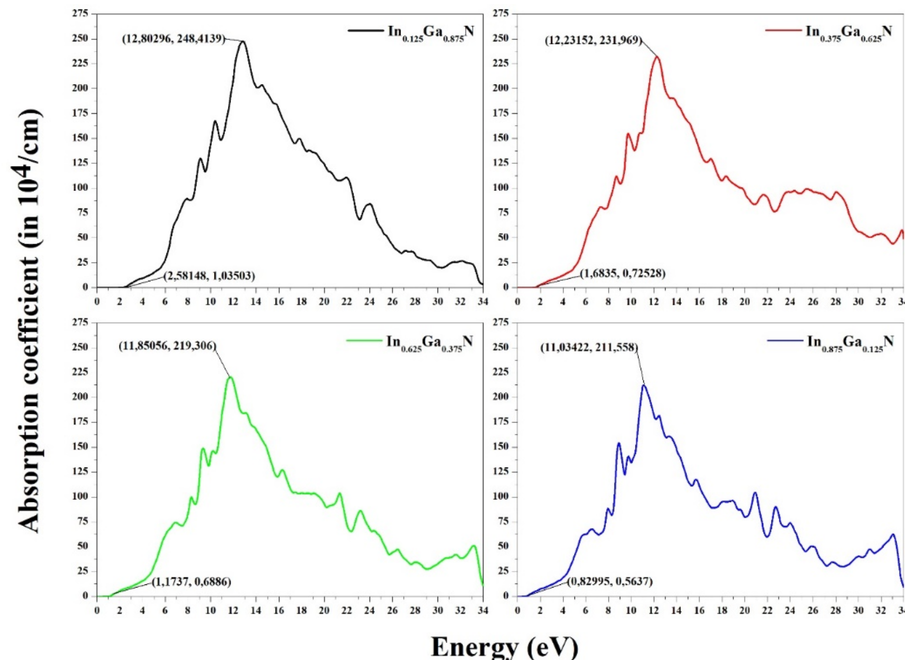

Figure 9. Absorption coefficient *α(ω)*for $In_{0,125}Ga_{0,875}\,N$, $In_{0,375}Ga_{0,625}\,N$, $In_{0,625}Ga_{0,375}\,N$ and $In_{0,875}Ga_{0,125}\,N$

4. CONCLUSIONS

Theoretical study of structural, electronic and optical properties of III-Nitrides alloys based on ‘‘FP-LAPW’’ calculation method, implementing LDA, GGA and mBJ approximations. These ternary compounds $In_{0,125}Ga_{0,875}\,N$, $In_{0,375}Ga_{0,625}\,N$, $In_{0,625}Ga_{0,375}\,N$ and $In_{0,875}Ga_{0,125}\,N$ have Wurtzite structure. The bandgaps nature of these materials is direct $\Gamma v - \Gamma c$. It is inferred that mBJ is an adequate theoretical method for the computation of the band structures of III/V materials. The findings require that mBJ will be a favorable potential for the bandgaps engineering of III/V compounds. In those alloys, the critical points in the optical spectra reveal the passage of electrons from valance band to the unoccupied states in the conduction band. The zero-frequency edge of $\varepsilon_1(0)$ and $n(0)$ show a reversed link with the bandgaps. From the interpretation of optical graphs, it is provided that those materials are implemented for optoelectronics components [In poor region (x less or equal 25%) of the $In_xGa_{1-x}N$] in ultraviolet energy ranges and for solar cells application.

Acknowledgements

The authors are grateful to the Directorate-General for Scientific Research and Technological Development (DGRSDT) for the supplied support to perform this research.

ORCID

Amina Benzina, https://orcid.org/0000-0002-9375-3006; **Abdel-Djawad Zebentout,** https://orcid.org/0000-0002-9503-7716
Lakhdar Benahmedi, https://orcid.org/0009-0008-0895-6820; **Taieb Seddik**, https://orcid.org/0000-0002-5777-1338
Hamza Abid, https://orcid.org/0000-0001-9647-7425

REFERENCES

[1] Liu, F., Wang, T., Gao, X., Yang, H., Zhang, Z., Guo, Y., ... & Wang, X. “Determination of the preferred epitaxy for III-nitride semiconductors on wet-transferred graphene,” Science Advances, **9**(31), eadf8484 (2023). https://doi.org/10.1016/j.commatsci.2024.113264

[2] G. Rehman, et al., “Electronic Band Structures of the Highly Desirable III-V Semiconductors: TB-mBJ DFT Studies,” J. Electron. Mater. **45**, 3314 (2016). https://doi.org/10.1007/s11664-016-4492-7

[3] Benbedra, A., Meskine, S., Boukortt, A., & Abbassa, H. “Polarization Properties of Wurtzite III-Nitride Alloys Using the Hexagonal Reference Structure,” ECS Journal of Solid-State Science and Technology, **12**(10), 103008 (2023). https://doi.org/10.1149/2162-8777/acfe9a

[4] B.-T. Liou, S.-H. Yen, and Y.-K. Kuo, “Vegard’s law deviation in band gaps and bowing parameters of the wurtzite III-nitride ternary alloys,” in: *Semiconductor Lasers and Applications II*, vol. 5628, edited by J.Q. Yao, Y.J. Chen, and S. Lee, (International Society for Optics and Photonics, SPIE, 2005), pp. 296–305, https://doi.org/10.1117/12.575300

[5] C.J. Praharaj, *Group III-Nitride Semiconductor Optoelectronics*, (John Wiley & Sons, 2023).
[6] M. Aslan, *et al*., "Structural and electronic properties of InN_xP_{1-x} alloy in full range ($0 \leq x \leq 1$)," Philosophical Magazine, **96**, 991 (2016). https://doi.org/10.1080/14786435.2016.1149248
[7] Chouchen, B., Ducroquet, F., Nasr, S., Alzahrani, A. Y., Hajjiah, A. T., & Gazzah, M. H. InxGa1-xN/GaN double heterojunction solar cell optimization for high temperature operation. Solar Energy Materials and Solar Cells, **234**, 111446 (2022). https://doi.org/10.1016/j.solmat.2021.111446
[8] Giorgi, G., Amato, M., Ossicini, S., Cartoixa, X., Canadell, E., & Rurali, R. "Doping of III–V arsenide and phosphide wurtzite semiconductors," The Journal of Physical Chemistry C, **124**(49), 27203-27212 (2020). https://dx.doi.org/10.1021/acs.jpcc.0c09391
[9] Imran, A., Sulaman, M., Yousaf, M., Anwar, M. A., Qasim, M., Dastgeer, G., ... & Wang, X. "Growth of High Mobility InN Film on Ga-Polar GaN Substrate by Molecular Beam Epitaxy for Optoelectronic Device Applications," Advanced Materials Interfaces, **10**(20), 2200105 (2023). https://doi.org/10.1002/admi.202200105
[10] Reilly, C. E., Keller, S., Nakamura, S., & DenBaars, S. P. "InN quantum dots by metalorganic chemical vapor deposition for optoelectronic applications," Frontiers in Materials, **8**, 647936 (2021). https://doi.org/10.3389/fmats.2021.647936
[11] H. Abboudi, H. EL Ghazi, R. En-nadir, M.A. Basyooni-M. Kabatas, A. Jorio, I. Zorkani, "Efficiency of InN/InGaN/GaN Intermediate-Band Solar Cell under the Effects of Hydrostatic Pressure, In-Compositions, Built-in-Electric Field, Confinement, and Thickness," Nanomaterials, **14**, 104 (2024). https://doi.org/10.3390/nano14010104
[12] R. Belghouthi, A. Rached, M. Aillerie, et al., "N-Face Semi-Bulk Absorber Boosts Conversion Efficiency of InGaN Solar Cell," J. Electron. Mater. **52**, 7566–7575 (2023). https://doi.org/10.1007/s11664-023-10662-w
[13] A. Bouadi, H. Naim, A. Djelloul, Y. Benkrima, R. Fares, "Enhancing the efficiency of the gallium indium nitride (InGaN) solar cell by optimizing the effective parameters," Chalcogenide Letters, **19**(9), 611-619 (2022). https://doi.org/10.15251/CL.2022.199.611
[14] Benahmedi, L., Besbes, A., & Djelti, R. "Structural, magnetic, elastic, and thermoelectric properties of Ba2InOsO6 double perovskite in the cubic phase: A DFT+ U study with spin-orbit-coupling," Journal of Magnetism and Magnetic Materials, **611**, 172629. (2024). https://doi.org/10.1016/j.jmmm.2024.172629
[15] Lakhdar, B., Anissa, B., Radouan, D., Al Bouzieh, N., & Amrane, N. "Structural, electronic, elastic, optical and thermoelectric properties of ASiCl3 (A= Li, Rb and Cs) chloroperovskites: a DFT study," Optical and Quantum Electronics, **56**(3), 313 (2024). https://doi.org/10.1007/s11082-023-06045-4
[16] L.C. de Carvalho, *et al*., "Ab initio calculation of optical properties with excitonic effects in wurtzite $In_xGa_{1-x}N$ and $In_xAl_{1-x}N$ alloys," Physical Review B, **87**, 195211 (2013). https://doi.org/10.1103/PhysRevB. 87.195211
[17] S. A. Hashemizadeh, and S. V. Mohammadi, "First-Principles Investigation of Density of States and Electron Density in Wurtzite $In_{0.5}Ga_{0.5}N$ Alloys with GGA-PBEsol Method," Journal of Nanostructures, **6**, 273 (2016) https://doi.org/10.22052/jns.2016.40758
[18] W.-W. Lin and Y.-K. Kuo, "Band structures and bandgap bowing parameters of wurtzite and zincblende III-nitrides," in: *Semiconductor Lasers and Applications*, vol. 4913, edited by Y. Luo and Y. Nakano, (International Society for Optics and Photonics, SPIE, 2002), pp. 236-247. https://doi.org/10.1117/12.482239
[19] N. N. Anua, *et al*., "DFT Investigations of the Optical Properties of Gallium Arsenide", in: *Advanced Materials Research*, vol. 895, (Trans. Tech. Publications Ltd, 2014), pp. 429–438, https://doi.org/10.4028/www.scientific.net/AMR.895.429
[20] K. Schwarz, and P. Blaha, "Solid state calculations using WIEN2k," Computational Materials Science, **28**, 259 (2003). https://doi.org/10.1016/S0927-0256(03)00112-5
[21] B. Amin, and I. Ahmad, "Theoretical investigation of half metallicity in Fe/Co/Ni doped ZnSe material systems," Journal of Applied Physics, **106**, 093710 (2009). https://doi.org/10.1063/1.3256186
[22] P. Hohenberg, and W. Kohn, "Inhomogeneous Electron Gas, Physical Review, **136**, B864 (1964). https://doi.org/10.1103/PhysRev.136.B864
[23] W. Kohn, and L. J. Sham, "Self-Consistent Equations Including Exchange and Correlation Effects," Physical Review, **140**, A1133 (1965). https://doi.org/10.1103/PhysRev.140.A1133
[24] M. Dadsetani, B. Kianisadr, and H. Nejatipour, "First Principles Investigation of the Optical Properties of BN_xP_{1-x} ($0 \leq x \leq 1$) Boron Ternary Alloys," J. Electron. Mater. **44**, 2699-2711 (2015). https://doi.org/10.1007/s11664-015-3691-y
[25] B.-T. Liou, and C.-W. Liu, "Electronic and Structural Properties of zincblende Al_xIn_{1-x}," Optics Communications, **274**, 361 (2007). https://doi.org/10.1016/j.optcom.2007.02.040
[26] B. Amin, et al., "Ab initio study of the bandgap engineering of $Al_{1-x}Ga_xN$ for optoelectronic applications," Journal of Applied Physics, **109**, 023109 (2011). https://doi.org/10.1063/1.3531996
[27] A. Benzina, *et al*., "First-principles calculation of structural, optoelectronic properties of the cubic $Al_xGa_yIn_{1-x-y}N$ quaternary alloys matching on AlN substrate, within modified Becke–Johnson (mBJ) exchange potential," Optik, **127**, 11577 (2016). https://doi.org/10.1016/j.ijleo.2016.09.014
[28] D. Koller, F. Tran, and P. Blaha, "Merits and limits of the modified Becke-Johnson exchange potential," Physical Review B, **83**, 195134 (2011). https://doi.org/10.1103/PhysRevB.83.195134
[29] M. B. Asfia, and M. A. Rashid, "First-Principles Study of Half Metallic Ferromagnetic and Optical Properties of Nb Doped Cubic ZnS using TB-mBJ Approximation," Dhaka University Journal of Science, **69**, 194–201 (2022). https://doi.org/10.3329/dujs.v69i3.60030
[30] S. Berri, "Theoretical analysis of the structural, electronic, optical and thermodynamic properties of trigonal and hexagonal $Cs_3Sb_2I_9$ compound," The European Physical Journal B, **93**, 1-12 (2020). https://doi.org/10.1140/epjb/e2020-10143-1
[31] V. Tyuterev, and N. Vast, "Murnaghan's equation of state for the electronic ground state energy," Computational Materials Science, **38**, 350 (2006). https://doi.org/10.1016/j. commatsci.2005.08.012
[32] R. Nunez-Gonzalez, *et al*., "First-principles calculation of the band gap of $Al_xGa_{1-x}N$ and $In_xGa_{1-x}N$," Revista Mexicana de fısica, **54**, 111 (2008). https://www.redalyc.org/pdf/570/57019061017.pdf
[33] S. Stepanov, *et al*., "Influence of Poisson's ratio uncertainty on calculations of the bowing parameter for strained InGaN layers," MRS Internet Journal of Nitride Semiconductor Research, **6**, e6 (2001). https://doi.org/10.1557/S1092578300000181

[34] A. I. Duff, L. Lymperakis, and J. Neugebauer, "Understanding and controlling indium incorporation and surface segregation on $In_xGa_{1-x}N$ surfaces: An ab initio approach," Physical Review B, **89**, 085307 (2014). https://doi.org/10.1103/PhysRevB.89.085307
[35] P. Rinke, *et al*., "Consistent set of band parameters for the group-III nitrides AlN, GaN, and InN," Physical Review B, **77**, 075202 (2008). https://doi.org/10.1103/PhysRevB.77.075202
[36] A. Belabbes, *et al*., "Cubic inclusions in hexagonal AlN, GaN, and InN: Electronic states," Physical Review B, **84**, 125108 (2011). https://doi.org/10.1103/PhysRevB.84.125108
[37] S.-H. Wei, *et al*., "Breakdown of the band-gap-common-cation rule: The origin of the small band gap of InN," Physical Review B, **67**, 165209 (2003). https://doi.org/10.1103/PhysRevB.67.165209
[38] Tian, Z., Zhang, P., Sun, W., Yan, B., & Sun, Z. "Vegard's law deviating Ti_2 (Sn_xAl_{1-x}) C solid solution with enhanced properties," Journal of Advanced Ceramics, **12**(8), 1655-1669 (2023). http://dx.doi.org/10.26599/JAC.2023.9220779
[39] E. Sakalauskas, *et al*., "Dielectric function and bowing parameters of InGaN alloys," Physica Status Solidi (b), **249**, 485 (2012). https://doi.org/10.1002/pssb.201100334
[40] Waack, J. M., Schäfer, N. A., Czerner, M., & Heiliger, C. "Structural, elastic, and electronic properties of cubic zinc-blende $In_xGa_{1-x}N$ alloys," Physical Review B, **110**(19), 195201 (2024). https://doi.org/10.1103/PhysRevB.110.195201
[41] M. O'Donnell, E.T. Jaynes, and J.G. Miller, "Kramers–Kronig relationship between ultrasonic attenuation and phase velocity," The Journal of the Acoustical Society of America, **69**, 696 (1981). https://doi.org/10.1121/1.385566
[42] Z.-Y. Jiao, S.-H. Ma, and Y.-L. Guo, "Simulation of optical function for phosphide crystals following the DFT band structure calculations," Computational and Theoretical Chemistry, **970**, 79 (2011). https://doi.org/10.1016/j.comptc.2011.05.030
[43] Resendiz-Hernandez, G., Leal-Perez, J. E., Herrera-Basurto, R., Mercader-Trejo, F. E., Auciello, O., & Hurtado-Macias, A. "Structural properties, bandgap, and complex dielectric function in Bi2Te3 thermoelectric by valence electron energy loss spectroscopy (VEELS) analysis," Journal of Alloys and Compounds, **965**, 171420 (2023). https://doi.org/10.1016/j.jallcom.2023.171420
[44] R. Ali, *et al*., "The structural, electronic and optical response of IIA–VIA compounds through the modified Becke–Johnson potential," Physica B: Condensed Matter, **410**, 93 (2013). https://doi.org/10.1016/j.physb.2012.09.050
[45] G. Murtaza, *et al*., "First principle study of cubic perovskites: AgTF3 (T=Mg, Zn)," Physica B: Condensed Matter, **406**, 4584 (2011). https://doi.org/10.1016/j.physb.2011.09.026
[46] A. Khettou, I. Zeydi, M. Chellali, M.B. Arbia, Mansouri, S., Helal, H., & Maaref, H. "Simulation and optimization of InGaN Schottky solar cells to enhance the interface quality," Superlattices and Microstructures, **142**, 106539 (2020). https://doi.org/10.1016/j.spmi.2020.106539

БАЗОВІ ДОСЛІДЖЕННЯ: ОПТОЕЛЕКТРОННІ ВЛАСТИВОСТІ СОНЯЧНИХ ЕЛЕМЕНТІВ НА ОСНОВІ СПЛАВУ ВЮРЦИТА InGaN В МЕЖАХ МОДИФІКОВАНОГО ОБМІННОГО ПОТЕНЦІАЛУ БЕКЕ-ДЖОНСОНА (MBJ)

Аміна Бензіна[a,b], Абдель-Джавад Зебентут[a,b], Лахдар Бенахмеді[c], Тайеб Седдік[d], Абдельхаді Лачабі[e], Хамза Абід[e]
[a]*Факультет наук і технологій (FST), Університет Айн-Темушент, 46000, Алжир*
[b]*Лабораторія прикладних матеріалів (AML), дослідницький центр, Джіллалі Ліабес, Університет Сіді-Бель-Аббес, Алжир*
[c]*Лабораторія технологій і властивостей твердих тіл, Університет Мостаганем Абдельхамід ібн Бадіс (UMAB), Алжир*
[d]*Лабораторія квантової фізики матерії та математичного моделювання (LPQ3M), факультет природничих наук і технологій, Мустафа Стамбулі Університет Маскара, Алжир*
[e]*Лабораторія прикладних матеріалів (AML), дослідницький центр, Джіллалі Ліабес, Університет Сіді-Бель-Аббес, Алжир*

Чисельне моделювання на основі розрахунків повної лінеаризованої розширеної плоскої хвилі (FP-LAPW) реалізовано в коді WIEN2K для вивчення фундаментальних структурних і оптоелектронних властивостей потрійної структури сплаву Wurtzite $In_xGa_{1-x}N$ (x = 0,125, 0,375, 0,625 і 0,875) узгоджено на підкладці GaN за допомогою 16-атомної суперкомірки. Узагальнене градієнтне наближення Ву та Коена, стандартний підхід локальної щільності та Тран-Блаха модифікований потенціал Бекке–Джонсона, були застосовані для покращення зонної структури та оптичних властивостей відповідних сполук. Коли це можливо, ми порівнюємо отримані результати за допомогою експериментів і обчислень, виконаних за різними обчислювальними схемами. У цих сплавах основні точки в оптичних спектрах відображають перехід електронів із валентної зони до незаповнених станів у зоні провідності. Результати свідчать про те, що потенціал Беке Джонсона буде багатообіцяючим потенціалом для розробки заборонених зон сполук III-V, які показали, що ці матеріали мають вирішальні коефіцієнти поглинання, які призводять до застосування для компонентів оптоелектроніки, особливо сонячних елементів.

Ключові слова: *повна потенційно-лінеаризована доповнена плоска хвиля (FP-LAPW); $In_xGa_{1-x}N$; Тран і Блаха модифікований потенціал Беке-Джонсона (TB-mBJ); вюрцит; сонячні елементи*